Photoproduction and Photon Structure at HERA

Katharina Müller

Physics Institute, University of Zurich, 8057 Zurich, Switzerland

DOI: http://dx.doi.org/10.3204/DESY-PROC-2009-03/Mueller

Many important QCD tests been performed with the experiments H1 and ZEUS at the HERA ep collider in the photoproduction regime. Differential cross sections of di-jets in photoproduction are shown in direct and resolved enhanced regions and different jet topologies and the sensitivity to different photon PDFs are studied. New results on prompt photons in photoproduction are presented. Further topics address the first measurement of diffractive scattering of quasi-real photons with large momentum transfer which is discussed in the BFKL framework and scaled momentum distributions of charged particles within jets.

1 Introduction

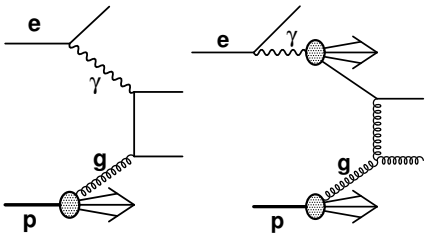

Figure 1: Examples of direct (left) and resolved (right) di-jet photoproduction diagrams in LO QCD.

High energy electron-proton scattering, as it has been carried out at the *ep* collider HERA, is dominated by so-called photoproduction processes, in which a beam lepton emits a quasi real photon which interacts with a parton from the proton. At leading order (LO) quantum chromodynamics (QCD) the scattering process may be classified into two basic types. In direct processes the entire photon interacts with a parton from the proton and there is no remnant in the photon direction, a typical LO diagram is shown in Fig. 1 (left).

In resolved processes, the incoming photon fluctuates into a partonic state out of which a parton with a momentum fraction x_γ participates in the hard scattering process as illustrated in Fig. 1 (right). There is a photon remnant carrying the fraction $1 - x_\gamma$ of the photon energy. Resolved processes are sensitive to the partonic structure of both the photon and the proton. At higher order in perturbative QCD (pQCD) the separation into two classes does not hold anymore.

The large statistics of the HERA data allows detailed tests of pQCD using hadronic jets and prompt (emerging from the hard interactions) photons. The hard scale is provided by the transverse energy E_T of the jet or the photon.

In this contribution recent results of di-jet and prompt photon production in photoproduction at HERA are discussed. In addition, some results with specific final states are presented: the diffractive production of photons with large momentum transfer and the multiplicity distribution of charged particles within jets.

2 Jets in Photoproduction

Experimentally, x_γ is estimated by x_γ^{obs}, which is reconstructed from the measurement of the transverse momenta E_T and pseudorapidities η[1] of the two jets, as

$$x_\gamma^{obs} = (E_T^{jet1} e^{-\eta(jet1)} + E_T^{jet2} e^{-\eta(jet2)})/(2yE_e).$$

Here, y is the inelasticity of the event and E_e the energy of the lepton beam. A pure LO direct process has $x_\gamma^{obs} = 1$ but initial and final state radiation as well as hadronisation may reduce it. Typically the resolved regime is defined to contain x_γ values below 0.75 or 0.8. The x_γ^{obs} distribution as measured in di-jet events, with $E_T^{jet1(2)} > 20(15)$ GeV and $-1 < \eta^{jet1,2} < 3$, is shown in Fig. 2 together with NLO predictions using five different parton density functions (PDFs) for the photon [1]. At high $x_\gamma^{obs} > 0.8$ the predictions are very similar as expected, since there is little sensitivity to the photon PDFs in this region, where towards low x_γ^{obs} the different PDFs vary by up to 70%. The prediction from CJK [2] deviates most from the others and does not describe the data, all other predictions describe the data within the experimental uncertainties.

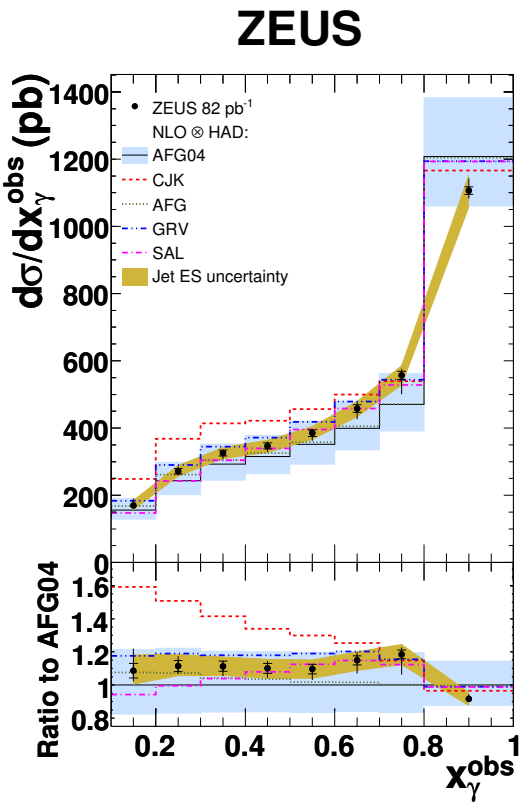

Figure 2: Measured cross section $d\sigma/dx_\gamma^{obs}$ compared with NLO QCD predictions with different PDFs for the photon. [1]

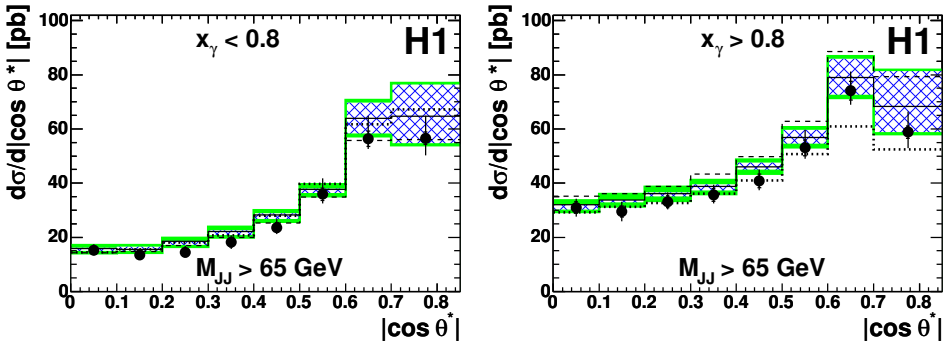

Figure 3: Di-jet cross section as a function of the cosine of the CMS scattering angle ($\cos\Theta^\star$) for a resolved (left) and direct (right) enriched sample [3].

[1]The pseudorapidity η is defined as $\eta = -\ln\tan(\theta/2)$, where θ is the polar angle with respect to the direction of the proton beam.

The concept of resolved and direct interactions of the photon can be tested by measuring the cross section as a function of $\cos\Theta^\star$, the cosine of the scattering angle in the centre of mass system (CMS). Statistically, direct interactions are dominated by quark propagators ($d\sigma/|d\cos\Theta^\star| \propto (1-|\cos\Theta^\star|)$), whereas the gluon propagator ($d\sigma/|d\cos\Theta^\star| \propto (1-|\cos\Theta^\star|)^{-2}$) dominates resolved interaction. Figure 3 shows the cross section as a function of $\cos\Theta^\star$ for di-jet events ($E_T^{jet1(2)} > 25(15)$ GeV and $-0.5 < \eta^{jet1,2} < 2.75$) with an invariant mass of the two jets larger than 65 GeV for a direct ($x_\gamma > 0.8$) and a resolved ($x_\gamma < 0.8$) enriched sample [3]. The cross section in the resolved enriched sample rises more rapidly with $\cos\Theta^\star$ than in the direct sample due to the dominating gluon propagator in the resolved sample.

Many more measurements of inclusive jet, di-jet and multijet production have been performed by the HERA experiments. In general data enriched with direct processes is well described by NLO QCD predictions, whereas resolved enhanced samples are less well described.

As an example, Fig. 4 [1] shows the transverse correlation of the two jets, $d\sigma/d|\Delta\Phi^{ij}|$, with $\Delta\Phi^{ij}$ being the azimuthal angle between the two jets, for x_γ^{obs} above and below 0.75. In the direct enhanced region, $x_\gamma^{obs} > 0.75$, the cross section falls steeply by three orders of magnitude, more steeply than for $x_\gamma^{obs} < 0.75$. The predictions from NLO QCD and the Monte Carlo (MC) generators HERWIG [4] and PYTHIA [5] are compared to the data. The MC predictions are normalised to the measured cross sections.

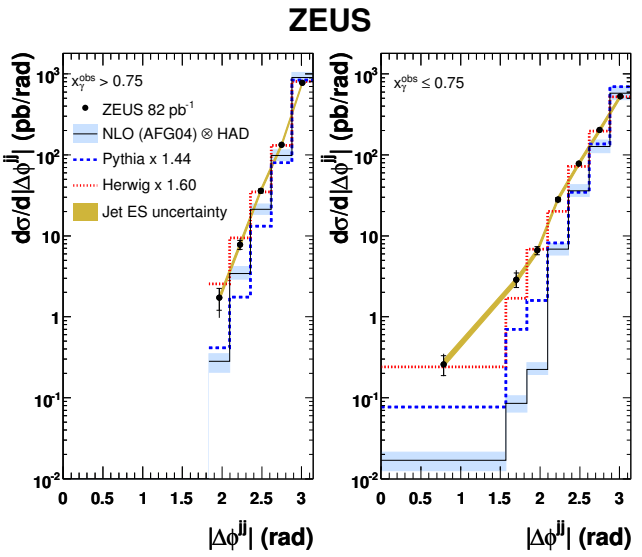

Figure 4: Measured cross section $d\sigma/d|\Delta\Phi^{ij}|$ for $x_\gamma^{obs} > 0.75$ (left) and $x_\gamma^{obs} \le 0.75$ (right). The measurement is compared to NLO predictions and to Monte Carlo predictions from HERWIG and PYTHIA [1].

At high x_γ^{obs}, NLO QCD agrees with data but it falls somewhat steeper, the PYTHIA prediction is very similar to NLO QCD, whereas HERWIG nicely describes the data. For low x_γ^{obs}, the NLO prediction is much too steep and significantly below the data except for the highest bin. Also the prediction from PYTHIA gives a poor description, HERWIG is in reasonable agreement with the data. This shows that the parton shower model as implemented in HERWIG gives a better description of higher order processes than PYTHIA.

As the pseudorapidities of the two jets are sensitive to the momentum distributions of the interacting partons, the cross sections as a function of x_p, the momentum fraction of the parton of the proton ($x_p = (E_T^{jet1} e^{\eta(jet1)} + E_T^{jet2} e^{\eta(jet2)})/(2E_p)$, with E_p the energy of the proton beam), are shown in Fig. 5 for $x_\gamma^{obs} > 0.8$ and two different jet topologies: in the left figure both jets are in the backward ($\eta^{jet1,2} < 1$), in the right figure, both jets are in the forward ($\eta^{jet1,2} > 1$) region [3]. The high x_p region can only be probed if both jets are pointing forward. The NLO QCD prediction describes the data well, except for the highest bin in x_p, where the

PDF uncertainty, indicated by the shaded area, is largest

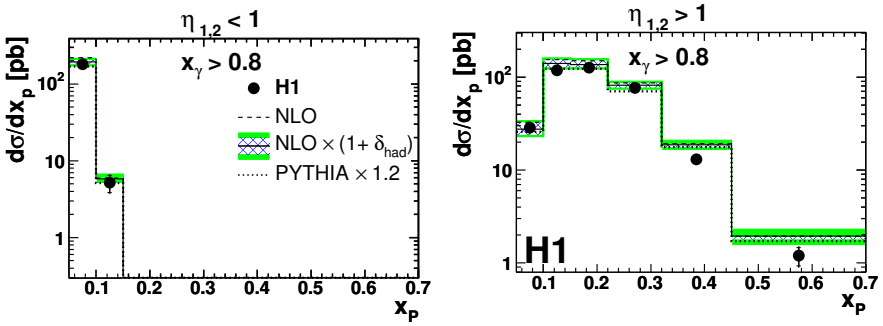

Figure 5: Cross section as a function of x_p for both jets pointing backwards (left) and forward (right). [3]

3 Prompt Photons in Photoproduction

Events with an isolated photon emerging from the hard subprocess $ep \to e\gamma X$ - so called prompt photons - offer an alternative access to study the hard interactions. The measurement with prompt photons require generally lower corrections for hadronisation than measurements relying on jets, since the photons emerge without the hadronisation process by which final state quarks or gluons form a jet. The analysis by H1 uses photoproduction data with an integrated luminosity of 340 pb^{-1}. Events are selected with an isolated photon with transverse energy $6 < E_T^\gamma < 15$ GeV and pseudorapidity $-1.0 < \eta^\gamma < 2.4$. For cross section measurements of prompt photons accompanied by a hadronic jet, the jet has to fulfil $4.5 < E_T^{jet}, -1.3 < \eta^{jet} < 2.3$. To ensure isolation of the photon, the photon has to carry more than 90% of the transverse energy of the jet in which it is contained, i.e. $z = E_T^\gamma / E_T^{photon-jet} > 0.9$. The isolation requirement rejects a large part from the background from decay photons of neutral hadrons. The photon signal is extracted from the sample which still contains background from the decay of neutral hadrons by a multivariate analysis which uses six different shower shape variables.

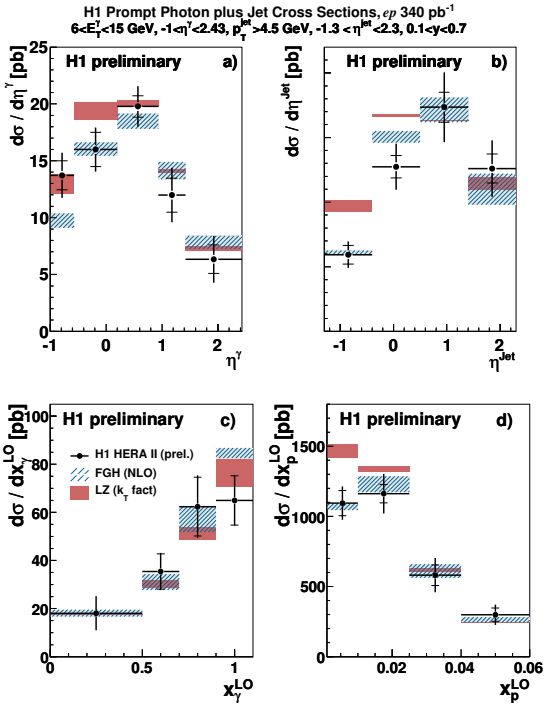

Figure 6: Differential cross sections for prompt photons with a hadronic jet $d\sigma/d\eta^\gamma$ (a), $d\sigma/d\eta^{jet}$ (b), $d\sigma/dx_\gamma^{LO}$(c) and $d\sigma/dx_p^{LO}$ (d).

Cross sections for the production of a prompt photon and a hadronic jet are presented in

Fig. 6 as a function of the variables η^γ, η^{jet}, x_γ^{LO} and x_p^{LO}, where

$$x_\gamma^{LO} = E_T^\gamma(e^{-\eta(\gamma)} + e^{-\eta(jet)})/(2yE_e) \text{ and } x_p^{LO} = E_T^\gamma(e^{\eta(\gamma)} + e^{\eta(jet)})/(2E_p).$$

At LO these definitions correspond to the longitudinal momentum fractions of the parton of the photon and the proton, respectively. The inner error bars correspond to the uncorrelated errors, including the statistical error, the outer error bars include the correlated errors added in quadrature. The results are compared to two sets of calculations, both corrected for hadronisation and multiple interaction effects: a next-to-leading order calculation by Fontannaz-Guillet-Heinrich (FGH) [6, 7] and a calculation based on the k_T-factorisation approach by Zotov-Lipatov (LZ) [8]. Both calculations give a reasonable description of the cross sections as a function of η^γ and x_γ^{LO} while only the NLO calculation well describes the cross sections as a function of η^{jet} of the associated hadronic jet and ${x_p}^{LO}$. Here, the LZ prediction is significantly too high for jets with $\eta^{jet} < 0.5$ which translates also in an overestimated cross section at low x_p. For the inclusive prompt photon measurements it is found that the NLO calculation is slightly below the data for backward photons ($\eta^\gamma < -0.06$). Both calculations have problems describing the transverse correlations between the photon and the jet which are sensitive to higher order effects. In general both calculations give a reasonable description of the different distributions but reveal problems in some kinematic regions.

4 Diffractive Scattering of high t Photons

Diffractive scattering of photons with large four-momentum transfer squared t,$\gamma p \to \gamma Y$, where Y is the proton dissociative system, was studied by H1 using an integrated luminosity of 46.2 pb^{-1} [9]. The analysis of high t photons complements the measurements of exclusive production of vector mesons, ρ, ϕ and J/Ψ [11], at HERA. For the production of photons the calculations are simplified by the absence of a vector meson wave function, it is an experimentally clean process and almost fully perturbatively calculable.

The study of exclusive diffractive processes in presence of a hard scale provides insight into the dynamics of the diffractive exchange. The four-momentum squared transferred at the proton vertex t, provides the relevant scale for the test of pQCD for $|t| >> \Lambda^2_{QCD}$. Diffractive photon scattering at high t can be modelled at sufficiently low values of Bjorken x in the leading log approximation (LLA) BFKL [10] model. Here, the gluon ladder couples to a single parton within the proton. The process is illustrated schematically in Figure 7.

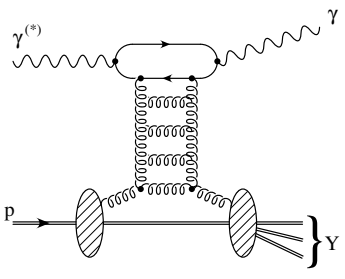

Figure 7: Schematic illustration of the process $\gamma p \to \gamma Y$ in a LLA BFKL approach

Due to the quasi-real nature of the incoming photon ($Q^2 < 0.01$ GeV^2), the transverse momentum of the final state photon, P_T^γ, is entirely transferred by the gluon ladder to the parton of the proton. The separation in rapidity between the parton scattered by the gluon ladder and the final state photon is given by $\Delta\eta \simeq log\hat{s}/(P_T^\gamma)^2)$, where $\hat{s}$ is the invariant mass of the incoming photon and the struck parton.

The data were recorded with the H1 detector during the running period 1999-2000 with an integrated luminosity of 46.2 pb^{-1}. Events are selected with a photon in the backward

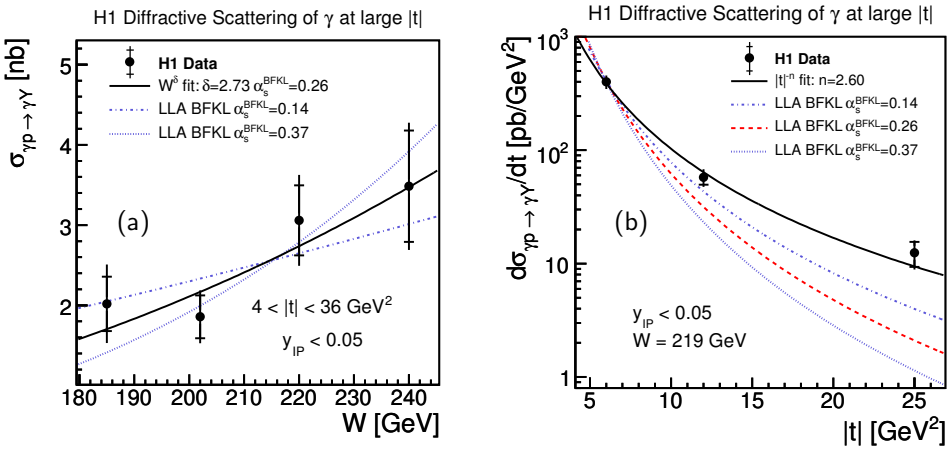

Figure 8: The γp cross section of diffractive scattering of photons as a function of W at $<|t|>= 6.1$ GeV^2 (a) and $|t|$ for $W = 219$ GeV^2 (b) [9].

calorimeter with $E_T^\gamma > 8$ GeV and a polar angle region $153° < \Theta < 177°$ and the scattered electron detected in the electron tagger, which restricts the virtuality of the incoming photon to $Q^2 < 0.01$ GeV^2. Diffractive events are selected by requiring that the event inelasticity $y_{I\!P} \simeq \Sigma_Y(E - P_z)/(2(E_e - E'_e)) < 0.05$ with E the energy and P_z the longitudinal momentum of a particle. The sum runs over all final state particles except the final state photon and the scattered electron. The cut on y_{IP} ensures a large rapidity gap between the photon and the proton dissociative system. The kinematic variable t reconstructs as $t = (P_T^\gamma)^2$ with a resolution of 11%. The γp centre of mass energy, W, is calculated from the energy of the scattered electron (E'_e) as $W \simeq \sqrt{1 - E'_e/E_e)s}$, where s is the ep centre of mass energy, with a relative resolution of 4%. These reconstructions are valid in the approximation of small scattering angles of the electron which is fulfilled for $Q^2 < 0.01$ GeV^2.

The $\gamma p \to \gamma Y$ cross section is shown in Figure 8 a) as a function of W for $4 < |t| < 36$ GeV^2. The cross section rises steeply with W which is usually interpreted as an indication of the presence of a hard sub-process in the diffractive interaction. A power-law dependence of the form $\sigma \propto W^\delta$ is fitted to the measured cross section. The δ value of $\delta = 2.73 \pm 1.02(\text{stat.})^{+0.56}_{-0.78}(\text{syst.})$ is compatible with the measurement for J/Ψ production. The data is also compared to predictions of the LLA BFKL model, using the HERWIG MC. The predictions are normalised to the measured cross section, as the normalisation is not predicted by the calculation. The W dependence can be used to measure α_s^{BFKL}, a free parameter in the theoretical prediction, which is the value of the strong coupling α_s used in the BFKL model. The W dependence is well described by the LLA BFKL prediction with $\alpha_s^{BFKL} = 0.26 \pm 0.10\ (\text{stat.})^{+0.05}_{-0.07}$ (syst.), as extracted from the fitted δ, using $\delta = 4(3\alpha_s/\pi)4ln2$. This value for α_s^{BFKL} is in agreement with the measurements using vector mesons.

The cross section as a function of $|t|$ is shown in Figure 8 b). It is compared to a fit of the form $d\sigma/dt \propto |t|^{-n}$. The fit yields $n = 2.60 \pm 0.19(\text{stat.})^{+0.03}_{-0.08}(\text{syst.})$. This $|t|$ dependence is significantly harder than measured for high $|t|$ diffractive photoproduction of J/Ψ mesons. The

BFKL model also predicts a too soft $|t|$ dependence and is unable to describe the data.

5 Scaled momentum distributions of charged particles

The measurement of soft charged particle distributions allows to study the formation of jets of hadrons which can be described as a convolution of parton showering and hadronisation. Parton showering can be calculated in pQCD as long as the energy scale is above Λ_{QCD} while hadronisation is a non perturbative process.

The study of charged particles with $P_T > 0.15$ GeV in jets was performed in di-jet events in photoproductionby the ZEUS collaboration using an integrated luminosity of 359 pb^{-1} [12].

The distributions are compared to predictions based on pQCD in the framework of the modified leading-logarithmic approximation (MLLA). Perturbative QCD based on the MLLA can be used to predict the multiplicity and momentum spectra of partons produced within cones centred on the initial parton direction. The MLLA may only be used to describe partons at scales above some minimum cutoff, $\Lambda_{\rm eff} > \Lambda_{\rm QCD}$. The value of $\Lambda_{\rm eff}$ is predicted to be independent of the process considered.

Figure 9 shows the number of charged particles as a function of $\xi = ln(1/x_{chp})$ where x_{chp} is the fraction of the jet momentum carried by the charged particle. The ξ distributions are shown for five bins in E_{jet} and three different cone opening angles Θ_c around the jet axis. The distributions are very similar and roughly Gaussian in shape with tails towards high ξ which corresponds to very low momentum particles.

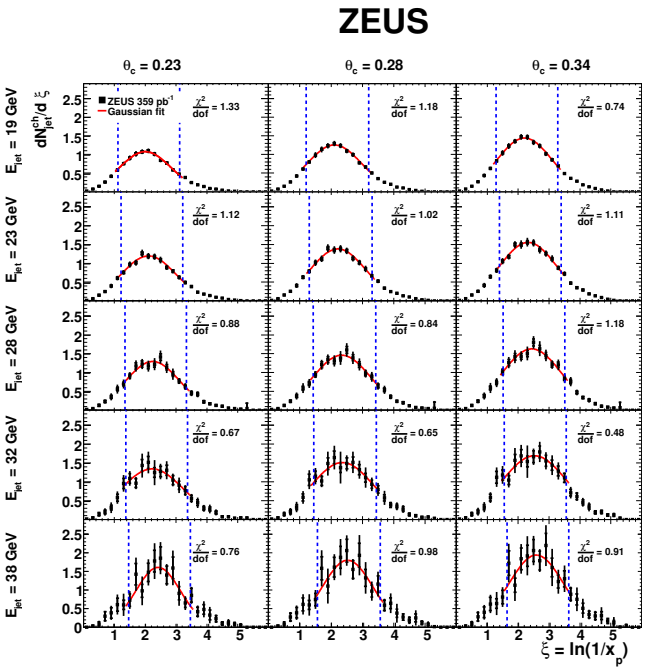

Figure 9: The ξ distribution for charged particles in jets for different bins in E_T of the jet and Θ_c the opening angle of the jet [12].

For each distribution, the peak position ξ_{peak} is extracted using a three-parameter Gaussian fit. The ξ_{peak} values for $\Theta_c = 0.23$ are shown in Fig. 10 as a function of $\mu \sin\Theta_c$, where the characteristic energy scale is $\mu = E_{jet}$. The peak value increases with the energy. The plot includes also results from ZEUS DIS [13], OPAL [14], TASSO [15], NOMAD [16] and CDF [17] at their characteristic energy scale. There is an approximately linear relationship between $\xi_{\rm peak}$ and $\ln(E_{\rm jet} \sin(\theta_c))$.

The MLLA predicts a small square-root correction to the linear dependence ($\xi^{\rm pl}_{\rm peak} = \frac{1}{2}Y + \sqrt{cY} + c$ with $c = 0.29$ and $Y = ln(\mu \sin(\Theta_c)/\Lambda_{eff})$. A single value of the intrinsic MLLA scale,

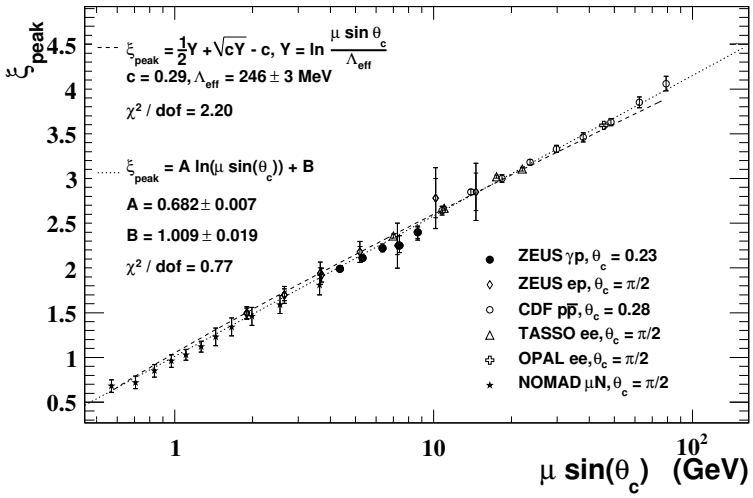

Figure 10: ξ_{peak} as a function of $\mu sin(\Theta_c)$, where μ is the characteristic energy scale for each specific process. The ZEUS γp data is shown together with ep, $p\bar{p}$ and e^+e^- data. The dashed line corresponds to the fit using the MLLA prediction [12].

$\Lambda_{\rm eff}$, is extracted by fitting the $\xi_{\rm peak}$ data according to the predicted relationship assuming $\Lambda_{\rm eff}$ is constant within the range of energies probed. The best fit value was found to be $\Lambda_{\rm eff} = 275 \pm 4({\rm stat.})^{+4}_{-8}({\rm syst.})$ MeV. The $\Lambda_{\rm eff}$ data are consistent with previously published data sets using different initial states, supporting the prediction that $\Lambda_{\rm eff}$ is universal.

6 Conclusions

Several measurements of jets and prompt photons in photoproduction have been presented. NLO calculations describe many aspects of jet samples which are dominated by direct interactions, whereas resolved enhanced samples are less well described. Prompt photon production in photoproduction is compared to a NLO calculation and to a calculation based on the k_T factorisation approach. Both calculation give a reasonable description of most of the distributions but reveal problems in some kinematic regions.

Diffractive scattering of photons at large momentum transfer was compared to predictions from a model based on the BFKL approach. While the W dependence of the cross section is well described, the data show a steeper t dependence than the model and and previous measurements with vector mesons.

The multiplicity distributions of charged particles within jets were measured and the intrinsic MLLA scale Λ_{eff} was extracted and found to be universal.

References

[1] S. Chekanov *et al.* [ZEUS Collaboration], Nucl. Phys. B **792** (2008) 1 [arXiv:0707.3749 [hep-ex]].

[2] F. Cornet, P. Jankowski and M. Krawczyk, Phys. Rev. D **70** (2004) 093004 [arXiv:hep-ph/0404063].

[3] A. Aktas *et al.* [H1 Collaboration], Phys. Lett. B **639** (2006) 21 [arXiv:hep-ex/0603014].

[4] G. Marchesini, B. R. Webber, G. Abbiendi, I. G. Knowles, M. H. Seymour and L. Stanco, Comput. Phys. Commun. **67** (1992) 465. G. Corcella *et al.*, JHEP **0101** (2001) 010 [arXiv:hep-ph/0011363].

[5] T. Sjostrand, P. Eden, C. Friberg, L. Lonnblad, G. Miu, S. Mrenna and E. Norrbin, Comput. Phys. Commun. **135** (2001) 238 [arXiv:hep-ph/0010017].
T. Sjostrand, Comput. Phys. Commun. **82** (1994) 74.

[6] M. Fontannaz, J. P. Guillet and G. Heinrich, Eur. Phys. J. C **21** 303 (2001) [arXiv:hep-ph/0105121].

[7] M. Fontannaz and G. Heinrich, Eur. Phys. J. C **34**, 191 (2004) [arXiv:hep-ph/0312009].

[8] A. V. Lipatov and N. P. Zotov, Phys. Rev. D **72** 054002 (2005) [arXiv:hep-ph/0506044].

[9] F. D. Aaron *et al.* [H1 Collaboration], Phys. Lett. B **672** (2009) 219 [arXiv:0810.3096 [hep-ex]].

[10] E. A. Kuraev, L. N. Lipatov and V. S. Fadin, Sov. Phys. JETP **45**, 199 (1977) [Zh. Eksp. Teor. Fiz. **72**, 377 (1977)].
I. I. Balitsky and L. N. Lipatov, Sov. J. Nucl. Phys. **28**, 822 (1978) [Yad. Fiz. **28**, 1597 (1978)].
L. N. Lipatov, Sov. Phys. JETP **63**, 904 (1986) [Zh. Eksp. Teor. Fiz. **90**, 1536 (1986)].

[11] S. Chekanov *et al.* [ZEUS Collaboration], Eur. Phys. J. C **26**, 389 (2003) [arXiv:hep-ex/0205081].
A. Aktas *et al.* [H1 Collaboration], Phys. Lett. B **638**, 422 (2006) [arXiv:hep-ex/0603038].
A. Aktas *et al.* [H1 Collaboration], Phys. Lett. B **568**, 205 (2003) [arXiv:hep-ex/0306013].
S. Chekanov *et al.* [ZEUS Collaboration], Eur. Phys. J. C **24**, 345 (2002) [arXiv:hep-ex/0201043].

[12] S. Chekanov *et al.* [ZEUS Collaboration], "Scaled momentum distributions of charged particles in dijet photoproduction at HERA", DESY-09-059, submitted to JHEP.

[13] M. Derrick *et al.* [ZEUS Collaboration], Z. Phys. C **67** (1995) 93 [arXiv:hep-ex/9501012].
J. Breitweg *et al.* [ZEUS Collaboration], Eur. Phys. J. C **11** (1999) 251 [arXiv:hep-ex/9903056].

[14] M. Z. Akrawy *et al.* [OPAL Collaboration], Phys. Lett. B **247** (1990) 617.

[15] W. Braunschweig *et al.* [TASSO Collaboration], Z. Phys. C **47** (1990) 187.

[16] J. Altegoer *et al.* [NOMAD Collaboration], Phys. Lett. B **445** (1999) 439.

[17] D. E. Acosta *et al.* [CDF Collaboration], Phys. Rev. D **68** (2003) 012003.